


Cascades of enstrophy and helicity in turbulence without vortex stretching

Tong Wu  and Wouter J. T. Bos *

Univ. Lyon, CNRS, Ecole Centrale de Lyon, INSA Lyon, Univ. Claude Bernard Lyon 1, LMFA, UMR5509, 69340 Ecully, France

 (Received 16 November 2021; accepted 12 August 2022; published 2 September 2022)

We consider three-dimensional turbulence from which vortex stretching is removed. Using direct numerical simulations, we show that in this system a dual cascade is observed, consisting of a forward enstrophy cascade and an inverse helicity cascade. In the inverse cascade range the energy spectrum scaling is proportional to $k^{-7/3}$, with k being the wave number. In the forward cascade range the spectrum is proportional to k^{-3} with a logarithmic correction.

DOI: [10.1103/PhysRevFluids.7.094601](https://doi.org/10.1103/PhysRevFluids.7.094601)

I. INTRODUCTION

The dynamics of two-dimensional (2D) and three-dimensional (3D) turbulent flows are very different. In 3D turbulence, energy is transferred mostly from the largest towards the smallest scales, with a spectrum proportional to $k^{-5/3}$ in the inertial subrange [1] (k being the wave number), and helicity is transferred in the same direction in scale space [2,3]. In 2D turbulence, energy and enstrophy exhibit a dual and counterdirectional cascade, i.e., energy flows towards large scales and enstrophy flows towards smaller ones. The inertial ranges corresponding to those inverse and forward cascades scale as $k^{-5/3}$ and k^{-3} , respectively [4,5].

An important difference between 2D and 3D flows can also be noted on the level of the governing equations. Formally, in both cases the dynamics of the vorticity $\boldsymbol{\omega}$ is governed by the curl of the Navier-Stokes equations,

$$\frac{\partial \boldsymbol{\omega}}{\partial t} + \mathbf{u} \cdot \nabla \boldsymbol{\omega} = \boldsymbol{\omega} \cdot \nabla \mathbf{u} + \nu \Delta \boldsymbol{\omega}, \quad (1)$$

where $\nabla \cdot \mathbf{u} = 0$, $\boldsymbol{\omega} = \nabla \times \mathbf{u}$, \mathbf{u} is the velocity, and ν is the kinematic viscosity. In the case of a two-dimensional flow, with velocity evolving in the plane perpendicular to the z axis, the vorticity is given by $\boldsymbol{\omega} = \omega \mathbf{e}_z$. In this case the vorticity is always perpendicular to the velocity gradients, so that the first term on the right-hand side of Eq. (1) is trivially zero. In two-dimensional flows the vortex stretching, the physical mechanism associated with this term, is thus equal to zero.

Vortex stretching is therefore often associated with the direct, forward energy cascade, and a vast body of literature has reported on the role of vortex stretching in 3D turbulence dynamics [6–16]. Studies on the importance of the vortex-stretching term, dissociating it from the influence of strain self-amplification, have given insights into the precise dynamical features associated with vortex stretching [10,11]. Further studies have reported on the decomposition of the stretching term into local and nonlocal contributions [12,13,15,16]. In these investigations, the dynamics of the Navier-Stokes equations are considered using either experiments [17], numerical simulation [13,18], or mathematical analysis [19], in order to understand how the interaction of strain and vorticity acts in a 3D flow.

*Corresponding author: wouter.bos@ec-lyon.fr

An alternative way to investigate the flow features associated with a given mechanism is to change the governing (Navier-Stokes) equations and to numerically or theoretically assess the modified equations and compare them with realistic flows. This method was used to investigate axisymmetric turbulence, a system in between two and three space dimensions [20–23]. In this system the vortex stretching is not zero, but its form is modified, leading to distinct behavior compared with 3D turbulence, with cascades towards both small and large scales [24–26].

In recent work this approach (modifying the governing equations) was extended to understand the role of vortex stretching in 3D turbulence, by removing the $\boldsymbol{\omega} \cdot \nabla \mathbf{u}$ term from Eq. (1). The first study of this system [27] allowed the discovery of an important difference between 2D turbulence and 3D turbulence without vortex stretching: In both systems, enstrophy is conserved; however, in the 3D system, energy is not conserved, and there is therefore no clear cascade of energy in that system. Subsequently, we showed [28] that helicity is a conserved quantity for 3D turbulence without vortex stretching. In this latter study, we assessed using statistical mechanics the truncated inviscid system and showed that the equilibrium distribution is importantly modified in the largest flow scales if helicity is present in the system. Following the reasoning of Kraichnan [4,29], this suggests that the system might have a tendency to transport helicity to large scales, unlike normal 3D turbulence.

The main motivation of the present investigation is to investigate this possibility of a dual cascade, by assessing the spectral dynamics and its associated fluxes in 3D turbulence without vortex stretching, using direct numerical simulations (DNSs). Indeed, in the previous investigations, inviscid relaxation was investigated by DNSs [28], and the forward enstrophy cascade was observed in closure theory [27]. The features of the present investigation are thus (i) validation by DNSs of the enstrophy cascade observed in closure theory, (ii) assessment and refinement of the scaling of the energy spectrum in the enstrophy cascade inertial range, (iii) the verification of a dual-cascade mechanism in the presence of helicity, and (iv) the proposition and assessment of scaling arguments for the inertial range of the inverse helicity cascade.

The rest of this paper is organized as follows. In Sec. II, we will predict the cascade directions and scaling of energy and helicity spectra in turbulence without vortex stretching. In Sec. III, we will present the numerical setup. Then, in Sec. IV we report on the assessment of the theoretical results. Finally, Sec. V concludes this investigation.

II. ANALYTICAL CONSIDERATIONS

In this section, we first recall recent results on the dynamics of inviscid turbulence without vortex stretching, obtained using statistical mechanics [28]. These results suggest a dual-cascade mechanism and give a prediction of the cascade directions of the two inviscid invariants in a turbulent system without vortex stretching: enstrophy and helicity. Then, using dimensional analysis, we propose predictions for energy and helicity spectra in the inertial ranges for a steady system.

A. Results from statistical mechanics

In Ref. [28] we considered the statistical mechanics of the incompressible Euler equations without vortex stretching,

$$\frac{\partial \boldsymbol{\omega}}{\partial t} + \mathbf{u} \cdot \nabla \boldsymbol{\omega} = 0, \quad (2)$$

with $\nabla \cdot \mathbf{u} = 0$. It was shown that this system conserves enstrophy W and helicity H defined as

$$W = \frac{1}{2} \langle \|\boldsymbol{\omega}\|^2 \rangle, \quad H = \frac{1}{2} \langle \mathbf{u} \cdot \boldsymbol{\omega} \rangle. \quad (3)$$

In contrast, kinetic energy, defined as

$$E = \frac{1}{2} \langle \|\mathbf{u}\|^2 \rangle, \quad (4)$$

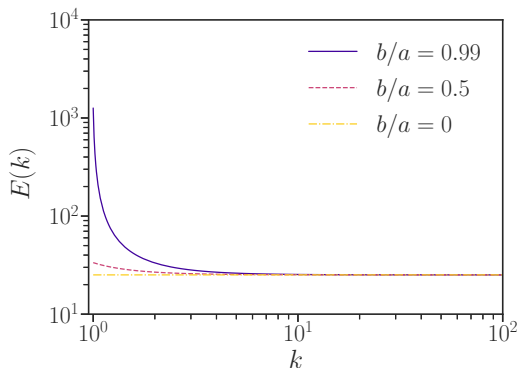


FIG. 1. Absolute equilibrium energy spectra as predicted by statistical mechanics [28]. The ratio b/a is associated with the amount of helicity in the system. In the absence of helicity ($b = 0$), the energy distribution is flat, corresponding to enstrophy equipartition. The presence of helicity, an invariant of the system, leads to a peaked energy distribution at the large scales.

is not conserved by Eq. (2). When projecting the dynamics of (2) on a truncated set of Fourier modes in three dimensions, the equilibrium energy, enstrophy, and helicity distributions can be determined [28], following the methods of Lee [30] and Kraichnan [4]. The so-obtained analytical predictions are

$$E(k) = \frac{8\pi ak^2}{a^2k^2 - b^2}, \quad (5)$$

$$H(k) = \frac{8\pi bk^2}{a^2k^2 - b^2}, \quad (6)$$

with k being the wave number and a, b being Lagrange multipliers determined by the values of the enstrophy, the helicity, and the range of considered wave vectors. Note that the spectra are defined such that

$$\int E(k)dk = E, \quad \int H(k)dk = H. \quad (7)$$

The enstrophy spectrum $W(k)$ is related to the energy spectrum by the relation

$$W(k) = k^2 E(k). \quad (8)$$

The equilibrium energy distribution [Eq. (5)] is shown in Fig. 1 for cases with and without helicity. This equilibrium energy distribution of the inviscid system allows us to formulate predictions of the cascade directions in the nonequilibrium (turbulent) case. The underlying idea is that a damped-driven system will evolve to approach the statistically most probable state, i.e., the equilibrium state.

We showed that excellent agreement was observed [28] between the equilibrium distributions (5) and the results of numerical integration of Eq. (2). The important feature of these equilibrium distributions with respect to the present investigation is that the presence of helicity leads to a modification of the energy distribution at the largest scales allowed by the system. Indeed, comparing the energy spectra in Fig. 1 with and without helicity, we observe the presence of a peak at $k = 1$, the smallest wave number. This shows that helicity, and the associated energy, has a tendency to concentrate in these scales. If helicity is injected in small scales, then we expect that nonlinear interactions will lead to a flux of helicity towards the large scales. The opposite is expected for enstrophy. Indeed, the equilibrium enstrophy spectrum is shown to be given by $W(k) \sim k^2$ for large k (and also for small k in the absence of helicity). If a dissipation mechanism is present at large wave numbers and enstrophy is initially concentrated at small wave numbers, the nonlinear

interactions are expected to have a tendency to redistribute the enstrophy towards large k in an attempt to restore equilibrium.

Note that these reasonings follow closely the ideas of Kraichnan on 2D turbulence [4], which suggested the existence of a dual cascade, with energy and enstrophy being transferred in opposite directions, and those for helicity transfer in classical 3D turbulence [29], suggesting a unique, forward cascade. In the present case we expect a similar picture to that in the 2D case, with enstrophy and helicity being transferred in opposite directions in scale space, and this will be checked numerically in Sec. IV.

B. Inertial range scaling

For turbulent systems with excitations on a wide range of scales, power spectra exhibit commonly self-similar ranges, where the considered quantity (e.g., the energy density) varies as a power law of the wave number. The most famous example is the inertial range of the kinetic energy spectrum in 3D turbulence, which scales as $E(k) \sim \epsilon^{2/3} k^{-5/3}$. This expression can be obtained by dimensional analysis, once we assume that the energy dissipation rate ϵ and the wave number k are the quantities determining the dynamics in the inertial range. As a matter of fact, ϵ appears in this expression since it is equal, at high Reynolds numbers and in a steady state, to the flux of energy through scale space from the injection scale to the dissipation range. In the present system, if a dual-cascade scenario is confirmed, the quantities determining the scaling of the energy, helicity, and enstrophy spectra will be the fluxes of enstrophy and helicity.

Let us consider the vorticity equation without vortex stretching, where we add an external force \mathbf{f} , acting at a given intermediate length scale k_f , and damping mechanisms \mathbf{d} , which act dominantly at large and small length scales, characterized by k_μ and k_ν , respectively:

$$\frac{\partial \boldsymbol{\omega}}{\partial t} + \mathbf{u} \cdot \nabla \boldsymbol{\omega} = \mathbf{f} - \mathbf{d}. \quad (9)$$

The left-hand side of this expression represents the nonlinear advection of vorticity. This term conserves the enstrophy and helicity of the system. Energy is not conserved and can be produced or destroyed by the interaction, somewhat like enstrophy which can be generated in classic three-dimensional turbulence. Therefore, if k_μ and k_ν are far enough removed from the forcing scale k_f , enstrophy and helicity should either pile up around k_f or be transferred to smaller or larger scales.

Following the reasoning in Sec. II A, we suppose that in a homogeneous turbulent flow governed by Eq. (9) at a sufficiently high Reynolds number, the statistics of the energy density in the inertial ranges have universal forms. For the forward enstrophy cascade and the inverse helicity cascade ranges, these universal forms are expected to be uniquely determined by the flux of enstrophy $\Pi_W(k)$ and helicity $\Pi_H(k)$, respectively. These fluxes are defined as

$$\Pi_W(k) = - \int_{\Sigma_k} \text{Re}[\hat{\mathbf{N}}(\mathbf{k}) \cdot \hat{\boldsymbol{\omega}}^*(\mathbf{k})] d\mathbf{k}, \quad (10)$$

$$\Pi_H(k) = - \int_{\Sigma_k} \text{Re}[\hat{\mathbf{N}}(\mathbf{k}) \cdot \hat{\mathbf{u}}^*(\mathbf{k})] d\mathbf{k}, \quad (11)$$

where $\mathcal{F}_{[\cdot]}$ and $\hat{\cdot}$ indicate Fourier transforms and $\text{Re}[\cdot]$ represents the real part of the quantity in brackets. Σ_k is the spherical domain in Fourier space consisting of all wave vectors with $\|\mathbf{k}\| \leq k$. The vorticity advection nonlinearity is indicated by

$$\hat{\mathbf{N}}(\mathbf{k}) = \mathcal{F}[-(\mathbf{u} \cdot \nabla)\boldsymbol{\omega}]. \quad (12)$$

By dimensional analysis, this hypothesis leads to the predictions for the inverse cascade range $k_\mu \ll k \ll k_f$,

$$E(k) \sim \Pi_H(k)^{2/3} k^{-7/3}, \quad (13)$$

$$H(k) \sim \Pi_H(k)^{2/3} k^{-4/3}, \quad (14)$$

and analogously for the forward cascade range $k_f \ll k \ll k_v$,

$$E(k) \sim \Pi_W(k)^{2/3} k^{-3}, \quad (15)$$

$$H(k) \sim \Pi_W(k)^{2/3} k^{-2}. \quad (16)$$

Expression (15) can be refined introducing logarithmic corrections, introduced by Kraichnan for inertial range scaling in 2D turbulence [31]. We recall the arguments of Kraichnan here.

It is expected that the flux of enstrophy in the forward cascade range is constant for large wave numbers. Physically, local transfer can be represented by an amount of enstrophy around a wave number k , which is transferred to smaller scales on a timescale $\tau(k)$,

$$\Pi_W(k) \sim \frac{k^3 E(k)}{\tau(k)}. \quad (17)$$

The typical timescale in the inertial range is associated with straining of the structures at scale k by structures at lower wave numbers. Such a straining time is of the order

$$\tau(k) \sim \left(\int_{k_f}^k p^2 E(p) dp \right)^{-1/2}. \quad (18)$$

Inserting a power law proportional to p^{-3} for the energy spectrum in expression (18) introduces directly a logarithmic dependence of $\tau(k)$ on the wave number. This leads therefore to a dependence of Eq. (17) on the wave number. Multiplying Eq. (15) by $[\ln(k/k_f)]^\gamma$ and substituting it into expressions (17) and (18), we find that for $\gamma = -1/3$, the flux becomes independent of the wave number. All these arguments, originally proposed for 2D turbulence, can be transposed directly to the current system, so that we expect that Eq. (15) can be refined to

$$E(k) \sim \Pi_W(k)^{2/3} k^{-3} [\ln(k/k_f)]^{-1/3}. \quad (19)$$

We expect the helicity spectrum in the enstrophy cascade range also to be affected by this correction.

All these scaling laws will be assessed using direct numerical simulation in Sec. IV. Note that we will not consider the helicity-free case in this paper. Indeed, for the mirror-symmetric case, $H(k)$ is trivially zero. Furthermore, in the absence of the inverse helicity cascade, the scales $k_\mu \ll k \ll k_f$ will display an equipartition of enstrophy, associated with an energy spectrum $E(k) \sim k^0$. This equilibrium scaling was assessed in Ref. [27] using closure and in Ref. [28] using DNS for the truncated inviscid system.

III. NUMERICAL METHOD AND SETUP

In Sec. IV, the results of numerical simulations are presented in order to assess the scaling properties of turbulence without vortex stretching. In the present section we detail the numerical setup we have used.

A. Forcing and damping of the system

The governing equation for the vorticity dynamics, Eq. (9), needs the specification of the forcing and damping terms. For the forcing term \mathbf{f} we choose an injection mechanism which keeps the energy constant in a narrow wave number range around wave number k_f . Note that this forcing method is widely used in investigations of 3D turbulence [32,33]. A convenient property of this type of forcing, with respect to the present investigation, is that it not only injects energy into the system, but also injects enstrophy and helicity.

The damping mechanism \mathcal{d} is somewhat more involved since we expect the establishment of a dual cascade. Let us first focus on the damping at the small scales of the system. The most obvious choice for the small-scale damping of a turbulent system is to use viscous dissipation. However, since we are concentrating on inertial range scaling without focusing too much on the dissipation range, we will attempt to reduce the size of the latter by using hyperviscosity. For classical 3D turbulence, we can increase the extent of the inertial range by an order of magnitude using this approach [34].

Similarly, when an inverse cascade is established, a damping term is required at the largest scales of the system, to be able to attain a steady state. Again, to limit the extent of the range influenced directly by this damping, we do not use a linear friction, but rather a hypofriction [35,36].

The equation that will be considered is

$$\frac{\partial \hat{\omega}}{\partial t} + \mathcal{F}[(\mathbf{u} \cdot \nabla)\omega] = \hat{f} - \nu k^{2\beta} \hat{\omega} - \mu k^{-2\alpha} \hat{\omega}, \quad (20)$$

with $\nabla \cdot \mathbf{u} = 0$. The left-hand side of this equation is the Fourier transform of the Euler equations without vortex stretching [Eq. (9)], and we discussed the equilibrium statistical mechanics of this system in Sec. II A. The terms on the right-hand side of this system allow us to consider the nonequilibrium features, by introducing forcing, the first term on the right-hand side, and damping at small and large scales, associated with the last two terms, respectively. Normal viscous dissipation corresponds to $\beta = 1$, and linear large-scale damping is obtained for $\alpha = 0$. In order to restrict the direct influence of the damping terms to a smaller wave number range, we use the values $\alpha = 1$ and $\beta = 4$, unless stated differently. The parameters ν and μ represent the hyperviscosity and hypofriction rate, respectively.

Using Eq. (20), we can define the dissipation of enstrophy as

$$\epsilon_W = \epsilon_W^v + \epsilon_W^\mu \quad (21)$$

$$= \int 2(\nu k^{2\beta} + \mu k^{-2\alpha}) k^2 E(k) dk. \quad (22)$$

We distinguish two contributions: ϵ_W^v , associated with the hyperviscous damping, and ϵ_W^μ , associated with the large-scale friction. Similarly, we define the contributions to the dissipation rate of helicity,

$$\epsilon_H = \epsilon_H^v + \epsilon_H^\mu \quad (23)$$

$$= \int 2(\nu k^{2\beta} + \mu k^{-2\alpha}) H(k) dk. \quad (24)$$

In the case of asymptotically large scale separation, $k_\mu \ll k_f \ll k_\nu$, we expect that the forward helicity flux and inverse enstrophy flux are negligible. In this case we will therefore have, for $k_f \ll k \ll k_\nu$ in a steady state,

$$\Pi_W(k) \approx \epsilon_W^v \quad (25)$$

and, for $k_\mu \ll k \ll k_f$,

$$\Pi_H(k) \approx -\epsilon_H^\mu. \quad (26)$$

In the present simulations we will verify to what extent these asymptotic relations are satisfied.

B. Characteristic length scales and measures of scale separation

The predictions in Sec. II B are supposed to be valid in inertial ranges, i.e., ranges of scales which are well separated from those scales where source and sink terms act. In order to observe clear scaling ranges, scale separation is thus required between the forcing scale k_f and the damping scales k_μ, k_ν . In studies of three-dimensional turbulence, an inertial range $k_f \ll k \ll k_\nu$ of about one decade in wave number can be observed in state-of-the-art numerical simulations. Dual cascades

need scale separation for two simultaneous ranges of wave numbers $k_\mu \ll k \ll k_f$ and $k_f \ll k \ll k_\nu$, and the physical constraints to observe clear dual-cascade behavior with well-developed scaling ranges for both cascades, simultaneously, require very large simulations. For instance, in 2D turbulence, resolutions of $(16\,384)^2$ grid points were needed to observe a hint of a dual cascade [37]. Whereas, in 3D turbulence, simulations on grids of 10^{12} grid points are nowadays possible [38], such simulations are extremely demanding with respect to numerical resources. It is therefore more convenient to investigate the two cascade ranges separately in individual simulations, by placing the forcing scale either close to k_μ or close to k_ν . This will be carried out in the following, and it will be shown that this approach allows us to accurately probe the inertial ranges of the system.

In the present simulations, the definition of a Reynolds number directly based on the values of ν and the large-scale velocity and integral length scale is not very informative, since we use hyperviscosity and hypofriction. In general the information associated with the Reynolds number which is most important when scaling is investigated is the scale separation between the large and small scales of the flow. We will therefore, instead of the classical Reynolds number, introduce a measure for the scale separation in the different flows.

For the forward cascade of enstrophy, the wave number representing the dissipative scales in a hyperviscous turbulence is given by [39] $k_\nu = (\epsilon_W^\nu / \nu_h^3)^{1/(6\beta)}$. Therefore the scale separation in the forward cascade range is represented by the ratio of this wave number and k_f , the wave number characterizing the forcing scale,

$$R_W = \frac{k_\nu}{k_f} = \frac{1}{k_f} \left(\frac{\epsilon_W^\nu}{\nu_h^3} \right)^{1/(6\beta)}. \quad (27)$$

We will use this kind of Reynolds number to characterize the scale separation in the forward cascade simulations.

Similarly, we can define a friction wave number $k_\mu = (\mu^3 / \epsilon_H^\mu)^{1/(6\alpha+1)}$. For the inverse cascade, we will choose the forcing scale to be as close as possible to the dissipation range and the scale k_μ where the friction acts to be as close as possible to the domain size. The scale separation is then characterized by the ratio of the forcing wave number k_f and the wave number k_μ . For this case we define, therefore,

$$R_H = \frac{k_f}{k_\mu} = k_f \left(\frac{\epsilon_H^\mu}{\mu^3} \right)^{1/(6\alpha+1)}, \quad (28)$$

which characterizes the extent of the scaling range in the inverse cascade.

The quantities R_W and R_H are thus not strictly Reynolds numbers, but dimensionless quantities which measure the scale separation in the forward cascade and inverse cascade range, respectively. We mention that in three-dimensional Navier-Stokes turbulence the Taylor-scale Reynolds number R_λ measures the scale separation in a similar way. In the presence of normal viscous dissipation, the ratio of the large (integral) scale L to the smallest (Kolmogorov) scale η is in that case given by $L/\eta \sim R_\lambda^{3/2}$.

C. Numerical method and resolution

All the simulations in this paper are performed using a standard pseudospectral solver with a third-order Adams-Bashforth time integration scheme [40], which was modified to remove vortex stretching [28]. The Biot-Savart operator is applied to Eq. (20) to obtain an equation for the velocity field. This velocity is kept incompressible by projecting the Fourier modes on a plane perpendicular to the wave vector.

Our computational domain is a cubic periodic box of size $L = 2\pi$. Aliasing errors are removed using the $2/3$ rule. DNSs are executed on grids of size 128^3 , 256^3 , and 512^3 to consider different values of R_W , R_H and thereby assess the robustness of the observed scaling ranges.

TABLE I. Numerical parameters for forward enstrophy cascade simulations.

Simulation cases	ν	β	k_ν	R_W	μ	α	Forcing
128^3	1×10^{-9}		19	12.67			$E(1) = 10^3$
256^3	$2^{-8} \times 10^{-9}$	4	38	25.33	0	0	$E(2) = 125$
512^3	$2^{-16} \times 10^{-9}$		75	50			$k_f = 1.5$

The values of the numerical parameters used for the different simulations are summarized in Tables I and II for the forward and inverse cascade simulations, respectively.

IV. NUMERICAL RESULTS

In this section we present the results of the numerical integration of Eq. (20). The choice of the forced wave number range and the values of μ and ν allows us to study inertial ranges for either the forward enstrophy cascade or the inverse cascade range associated with helicity transfer.

A. Forward enstrophy cascade

We start by forcing the largest scales of the system: The energy in the largest scales is kept constant in time. In the wave number range $1 \leq k \leq 1.5$ the energy is given a value $E(1) = 10^3$, and for $1.5 < k \leq 2.5$ the energy level is kept at a value $E(2) = 125$. In the simulations the flow attains a statistically steady state where the enstrophy injected in the forcing range is in equilibrium with the enstrophy dissipated by the hyperviscous damping term. Since no scales larger than the forcing scale are available in our domain, no inverse cascade can be established, and no large-scale damping is needed to allow for a steady state. The value of μ is therefore chosen to be zero in these simulations.

In Figs. 2(a) and 2(b) we show energy and helicity spectra, respectively. The insets show their compensated spectra. For the energy spectrum, we can observe that an inertial range is present, with a wave-number dependence close to k^{-3} , as was also observed in the two-point closure investigation [27]. Similarly, for the helicity spectrum, the exponent is close to k^{-2} .

In the inset of Fig. 2(a) we show the energy spectra premultiplied by k^3 . The inset illustrates that for the largest k , before the dissipation rate is reached, the spectra are approximately flat. The plateau is, however, absent for smaller k . We show in the same inset how a logarithmic correction [cf. Eq. (19)] allows us to improve the agreement with the predictions for these scales.

In order to assess that these scaling ranges correspond to constant-flux solutions, we compute the enstrophy flux, defined in Eq. (10). In Fig. 2(c), it is observed that a substantial range of wave numbers is observed where the flux is almost constant and approximately equal to ϵ_W^ν . Since the first two modes of the system are forced, there is no space for an inverse cascade to form.

TABLE II. Numerical parameters for inverse helicity cascade simulations. The energy in the forced-wave-number shells is kept at a constant value $E(k_f^{(1)}) = E(k_f^{(2)}) = 10^{-3}$. The forcing wave number is defined as $k_f = (k_f^{(1)} + k_f^{(2)})/2$.

Simulation cases	ν	β	μ	α	k_μ	R_H	$k_f^{(1)}; k_f^{(2)}$
128^3	256×10^{-13}				1.127	13.75	15; 16
256^3	10^{-13}	4	0.45	1	0.854	35.71	30; 31
512^3	$\frac{1}{256} \times 10^{-13}$				0.648	93.36	60; 61

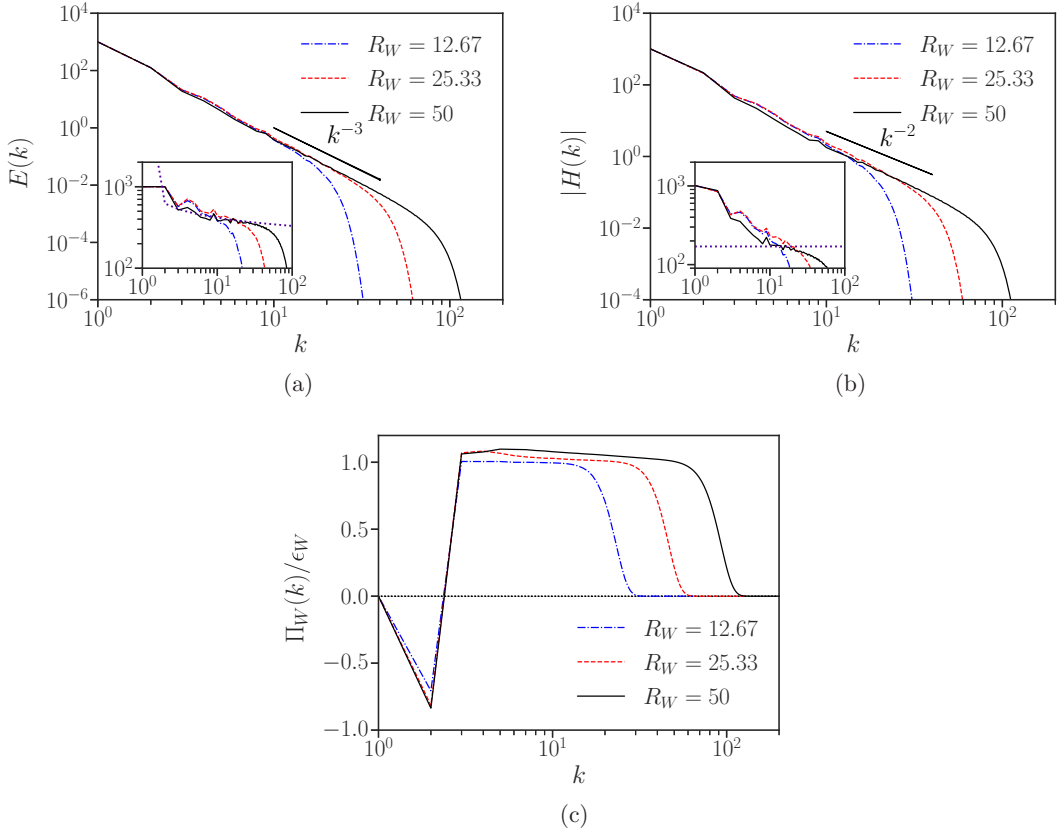


FIG. 2. Spectra of energy, helicity, and flux for the forward enstrophy cascade at different values of the scale-separation number R_W . (a) Energy spectra. The inset shows compensated spectra $k^3 E(k)$, and the dotted line in the inset indicates the logarithmic correction [see Eq. (19)]. (b) Helicity spectra. Inset: compensated spectra $|k^2 H(k)|$. (c) Flux of enstrophy, normalized by the hyperviscous dissipation of enstrophy ϵ_W .

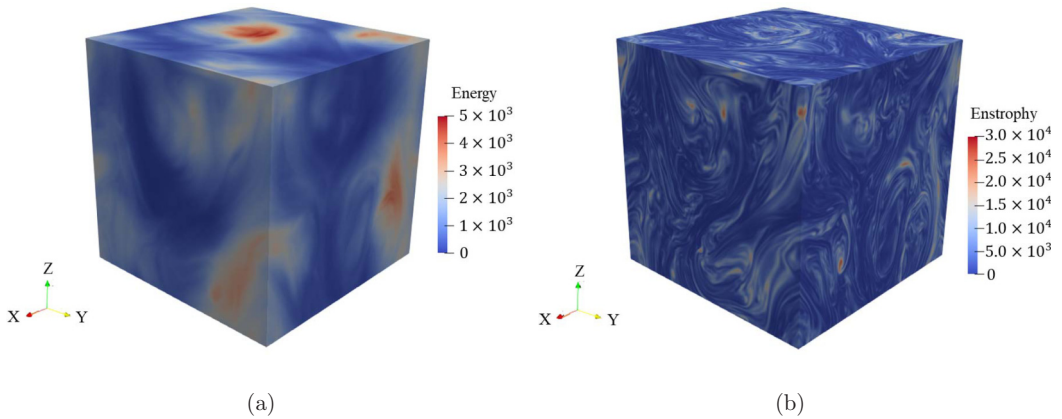


FIG. 3. Visualizations of the no-vortex-stretching system forced at large scales for the 512^3 case ($R_W = 50$). (a) Energy. (b) Enstrophy.

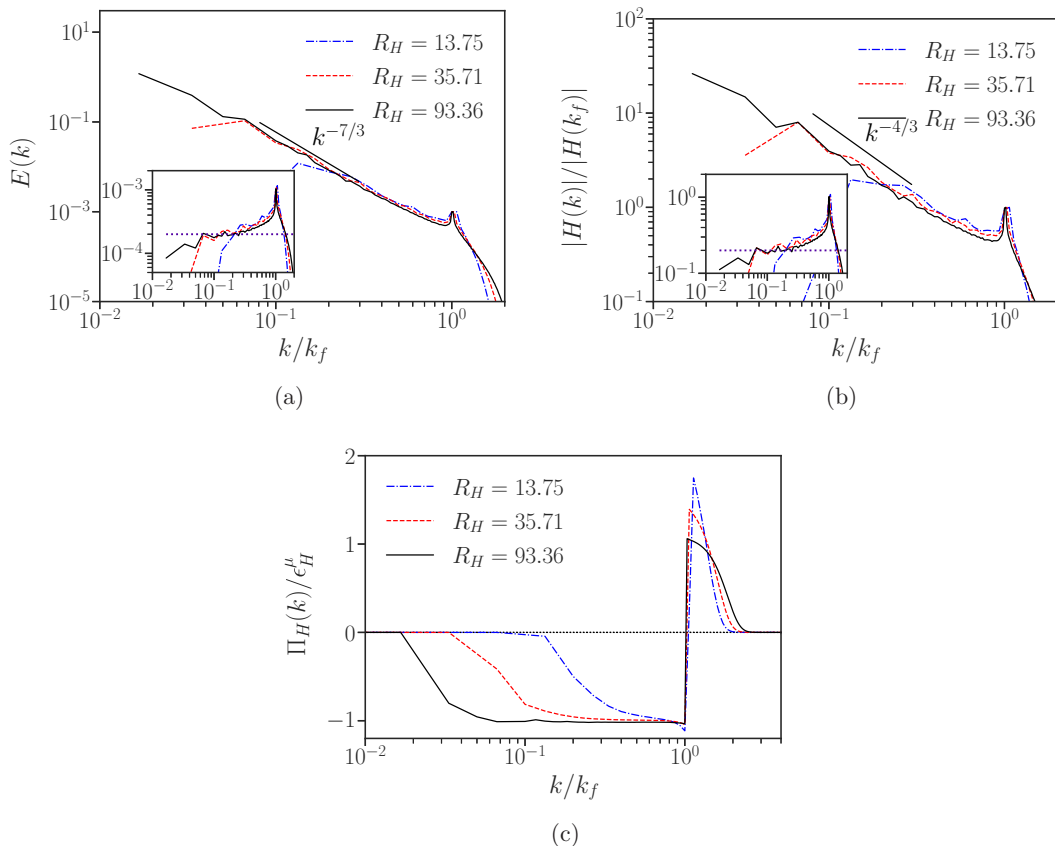


FIG. 4. Wave-number spectra for the inverse helicity cascade regime at different values of the scale-separation number R_H . (a) Energy spectra, (b) helicity spectra, and (c) helicity flux spectra. The insets in (a) and (b) show compensated spectra $(k/k_f)^{7/3}E(k)$ and $(k/k_f)^{4/3}|H(k)|/|H(k_f)|$, respectively.

In Fig. 3, enstrophy and energy are visualized for the simulation at the largest resolution. The energy plot shows large-scale structures at the forcing scale. The enstrophy shows more fine-grained filamentary structures.

B. Inverse helicity cascade

After the confirmation of the predictions for the forward cascade of enstrophy in the last section, we now turn to the assessment of the inverse cascade, associated with helicity conservation. We consider the same numerical scheme but change the forcing range to higher wave numbers. We carry out simulations at resolutions of 128^3 , 256^3 , and 512^3 associated with three values of the scale-separation parameter R_H . The corresponding forcing scales are now $k_f = 15.5$, 30.5 , and 60.5 , respectively, for the three considered resolutions.

For all simulations, hyperviscosity and hypofriction are used to render the system stationary. The numerical parameters are given in Table II. Energy and helicity spectra during the steady state are shown in Figs. 4(a) and 4(b), respectively. We can observe that in the inertial range, the spectral exponent approaches the predictions of Sec. II B, in particular, for the largest resolution considered here.

The physical picture is further confirmed in Fig. 4(c), which shows the helicity fluxes, normalized by the hypofriction dissipation rate. It is observed that the flux attains the value of the large-scale

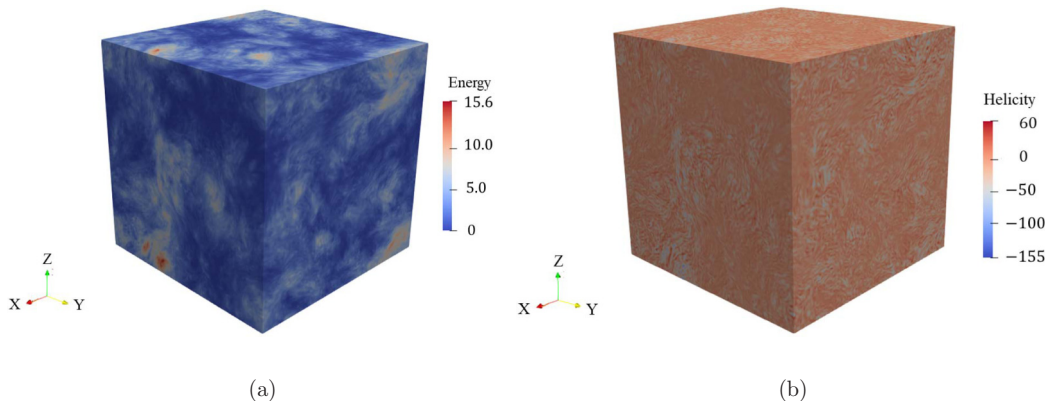


FIG. 5. Visualizations of the no-vortex-stretching system forced at small scales for $R_W = 93$. (a) Kinetic energy. (b) Helicity.

dissipation ϵ_H^μ for $k < k_f$. For the largest resolution a constant flux is observed for more than one decade in wave numbers.

The spatial kinetic energy distribution and helicity distributions are visualized in Fig. 5. We observe that the mean value of the helicity is not zero, but no outstanding large-scale helical features are observed. Clearly, the large-scale friction does prevent the system from generating energetic, helical structures at the box scale.

V. CONCLUSIONS

We have in this paper illustrated the cascades of enstrophy and helicity, as well as their associated spectral scalings in isotropic three-dimensional turbulence without vortex stretching. Confirming the predictions from statistical mechanics [28], we showed that enstrophy cascades from large scales towards small scales, where it is dissipated, while helicity is transferred from small scales towards large scales.

In the inertial range of the forward cascade, energy and helicity spectra follow $E(k) \propto k^{-3}$ and $|H(k)| \propto k^{-2}$ for $k \gg k_f$, associated with a conserved enstrophy flux towards large k . Closer to the forcing scale, logarithmic corrections allow us to describe the deviation of the spectral energy distribution from the dimensional prediction.

For the inverse cascade, we observe the scalings $E(k) \propto k^{-7/3}$ and $|H(k)| \propto k^{-4/3}$ for wave numbers in the range between the friction wave number and the forcing wave number. It is shown that these wave number ranges are associated with a constant (conserved) flux of helicity towards small k .

An interesting perspective of the present investigation would be the assessment of the chirality of the flow structures. Indeed, it is observed that in our simulations the relation between helicity and energy spectra is nearly $|H(k)| = kE(k)$. Formulations of energy and helicity using the helical decomposition [29] allow us to show that $|H(k)| = kE(k)$ corresponds to homochiral modes. In flows where only a certain class of chiral modes is retained, a dual cascade is observed, with an energy spectrum proportional to $k^{-7/3}$, associated with helicity conservation [41]. The interesting feature is that in that particular case, the helicity is transferred to small scales as opposed to the inverse helicity cascade in the present system.

Another feature of this system which deserves further research is the long-time evolution of the system in the absence of large-scale damping. Indeed, in the absence of friction or other forms of large-scale damping, helicity will pile up, as energy does for two-dimensional turbulence. How such a condensate manifests itself and changes the dynamics of the present system is an open question.

Furthermore, since the system resembles two-dimensional turbulence in certain aspects, the characterization of flow structures using statistical mechanics [42,43] might be an interesting direction for investigation.

ACKNOWLEDGMENTS

We acknowledge the China Scholarship Council (CSC) for financial support. All simulations were carried out using the facilities of the PMCS2I (École Centrale de Lyon).

-
- [1] A. N. Kolmogorov, The local structure of turbulence in an incompressible viscous fluid with very large Reynolds numbers, *Dokl. Akad. Nauk SSSR* **30**, 301 (1941); Reprinted in *Proc. R. Soc. London Ser. A* **434**, 9 (1991).
 - [2] J. C. André and M. Lesieur, Influence of helicity on the evolution of isotropic turbulence at high Reynolds number, *J. Fluid Mech.* **81**, 187 (1977).
 - [3] V. Borue and S. A. Orszag, Spectra in helical three-dimensional homogeneous isotropic turbulence, *Phys. Rev. E* **55**, 7005 (1997).
 - [4] R. H. Kraichnan, Inertial ranges in two-dimensional turbulence, *Phys. Fluids* **10**, 1417 (1967).
 - [5] C. E. Leith, Diffusion approximation for two-dimensional turbulence, *Phys. Fluids* **11**, 671 (1968).
 - [6] H. Tennekes and J. L. Lumley, *A First Course in Turbulence* (MIT Press, Cambridge, MA, 1972).
 - [7] P. A. Davidson, *Turbulence: An Introduction for Scientists and Engineers* (Oxford University Press, Oxford, 2004).
 - [8] G. I. Taylor, The spectrum of turbulence, *Proc. R. Soc. London A* **164**, 476 (1938).
 - [9] T. Leung, N. Swaminathan, and P. A. Davidson, Geometry and interaction of structures in homogeneous isotropic turbulence, *J. Fluid Mech.* **710**, 453 (2012).
 - [10] P. L. Johnson, Energy Transfer from Large to Small Scales in Turbulence by Multiscale Nonlinear Strain and Vorticity Interactions, *Phys. Rev. Lett.* **124**, 104501 (2020).
 - [11] M. Carbone and A. D. Bragg, Is vortex stretching the main cause of the turbulent energy cascade? *J. Fluid Mech.* **883**, R2 (2020).
 - [12] P. E. Hamlington, J. Schumacher, and W. J. A. Dahm, Local and nonlocal strain rate fields and vorticity alignment in turbulent flows, *Phys. Rev. E* **77**, 026303 (2008).
 - [13] D. Buaria, A. Pumir, and E. Bodenschatz, Self-attenuation of extreme events in Navier-Stokes turbulence, *Nat. Commun.* **11**, 5852 (2020).
 - [14] D. Buaria, E. Bodenschatz, and A. Pumir, Vortex stretching and enstrophy production in high Reynolds number turbulence, *Phys. Rev. Fluids* **5**, 104602 (2020).
 - [15] G. L. Eyink, Locality of turbulent cascades, *Phys. D (Amsterdam)* **207**, 91 (2005).
 - [16] K. K. Nomura and G. K. Post, The structure and dynamics of vorticity and rate of strain in incompressible homogeneous turbulence, *J. Fluid Mech.* **377**, 65 (1998).
 - [17] B. Lüthi, A. Tsinober, and W. Kinzelbach, Lagrangian measurement of vorticity dynamics in turbulent flow, *J. Fluid Mech.* **528**, 87 (2005).
 - [18] J. G. Ballouz and N. T. Ouellette, Tensor geometry in the turbulent cascade, *J. Fluid Mech.* **835**, 1048 (2018).
 - [19] *An Informal Conceptual Introduction to Turbulence*, edited by A. Tsinober, Fluid Mechanics and Its Applications, Vol. 92 (Springer, Dordrecht, 2009).
 - [20] N. Leprovost, B. Dubrulle, and P. H. Chavanis, Dynamics and thermodynamics of axisymmetric flows: Theory, *Phys. Rev. E* **73**, 046308 (2006).
 - [21] R. Monchaux, P. P. Cortet, P. H. Chavanis, A. Chiffaudel, F. Daviaud, P. Diribarne, and B. Dubrulle, Fluctuation-Dissipation Relations and Statistical Temperatures in a Turbulent von Kármán Flow, *Phys. Rev. Lett.* **101**, 174502 (2008).
 - [22] A. Naso, R. Monchaux, P. H. Chavanis, and B. Dubrulle, Statistical mechanics of Beltrami flows in axisymmetric geometry: Theory reexamined, *Phys. Rev. E* **81**, 066318 (2010).

- [23] B. Qu, W. J. T. Bos, and A. Naso, Direct numerical simulation of axisymmetric turbulence, *Phys. Rev. Fluids* **2**, 094608 (2017).
- [24] E. Herbert, F. Daviaud, B. Dubrulle, S. Nazarenko, and A. Naso, Dual non-Kolmogorov cascades in a von Kármán flow, *Europhys. Lett.* **100**, 44003 (2012).
- [25] B. Qu, A. Naso, and W. J. T. Bos, Cascades of energy and helicity in axisymmetric turbulence, *Phys. Rev. Fluids* **3**, 014607 (2018).
- [26] Z. Qin, H. Faller, B. Dubrulle, A. Naso, and W. J. T. Bos, Transition from non-swirling to swirling axisymmetric turbulence, *Phys. Rev. Fluids* **5**, 064602 (2020).
- [27] W. J. T. Bos, Three-dimensional turbulence without vortex stretching, *J. Fluid Mech.* **915**, A121 (2021).
- [28] T. Wu and W. J. T. Bos, Statistical mechanics of the Euler equations without vortex stretching, *J. Fluid Mech.* **929**, A11 (2021).
- [29] R. H. Kraichnan, Helical turbulence and absolute equilibrium, *J. Fluid Mech.* **59**, 745 (1973).
- [30] T. D. Lee, On some statistical properties of hydrodynamical and magnetohydrodynamical fields, *Q. Appl. Math.* **10**, 69 (1952).
- [31] R. H. Kraichnan, Inertial-range transfer in two- and three-dimensional turbulence, *J. Fluid Mech.* **47**, 525 (1971).
- [32] S. Chen, G. D. Doolen, R. H. Kraichnan, and Z. She, On statistical correlations between velocity increments and locally averaged dissipation in homogeneous turbulence, *Phys. Fluids A* **5**, 458 (1993).
- [33] L. P. Wang, S. Chen, J. G. Brasseur, and J. C. Wyngaard, Examination of hypotheses in the Kolmogorov refined turbulence theory through high-resolution simulations. Part 1. Velocity field, *J. Fluid Mech.* **309**, 113 (1996).
- [34] V. Borue and S. A. Orszag, Forced three-dimensional homogeneous turbulence with hyperviscosity, *Europhys. Lett.* **29**, 687 (1995).
- [35] V. Borue, Inverse Energy Cascade in Stationary Two-Dimensional Homogeneous Turbulence, *Phys. Rev. Lett.* **72**, 1475 (1994).
- [36] W. J. T. Bos and J. P. Bertoglio, Large scale bottleneck effect in two-dimensional turbulence, *J. Turbul.* **10**, N30 (2009).
- [37] G. Boffetta, Energy and enstrophy fluxes in the double cascade of two-dimensional turbulence, *J. Fluid Mech.* **589**, 253 (2007).
- [38] T. Ishihara, K. Morishita, M. Yokokawa, A. Uno, and Y. Kaneda, Energy spectrum in high-resolution direct numerical simulations of turbulence, *Phys. Rev. Fluids* **1**, 082403(R) (2016).
- [39] A. G. Lamorgese, D. A. Caughey, and S. B. Pope, Direct numerical simulation of homogeneous turbulence with hyperviscosity, *Phys. Fluids* **17**, 015106 (2005).
- [40] A. Delache, C. Cambon, and F. Godeferd, Scale by scale anisotropy in freely decaying rotating turbulence, *Phys. Fluids* **26**, 025104 (2014).
- [41] L. Biferale, S. Musacchio, and F. Toschi, Split energy–helicity cascades in three-dimensional homogeneous and isotropic turbulence, *J. Fluid Mech.* **730**, 309 (2013).
- [42] R. Robert and J. Sommeria, Statistical equilibrium states for two-dimensional flows, *J. Fluid Mech.* **229**, 291 (1991).
- [43] J. Miller, Statistical Mechanics of Euler Equations in Two Dimensions, *Phys. Rev. Lett.* **65**, 2137 (1990).